JOTCS A Journal of the Turkish Chemical Society Section: A Chemistry

TURKISH CHEMICAL SOCIETY

Microstructure-Mechanical Properties of Mg-xCa Alloys Produced by Mechanical Alloying-Hot Pressing Process and Their Optimization Using Central Composite Design Method

Lütfiye Feray Güleryüz[1*], Rasim İpek[1]

[1]Department of Mechanical Engineering, Faculty of Engineering Ege University, Bornova, 35040, İzmir, Türkiye.

Abstract: In the study, Mg-xCa alloys with high mechanical performance were developed using a statistical model central composite design (CCD) method to predict the mechanical properties of Mg and Ca powders produced by powder metallurgy. Powder metallurgy (TM) is a production method that offers great advantages over other production methods. However, there are limited studies in the literature on the production of alloying Ca to eliminate the high degradation rate of pure Mg loss. Mg and Ca powders were subjected to the alloying process for different times as 11.99-14.43-18-21.5-24 h, and after mechanical alloying (MA), grain size measurements of the powders and XRD and SEM-EDS analyses were performed. After MA, the powders were sintered at different temperatures, such as 325-370-437-504-549°C in an argon gas environment under 46 MPa pressure, and samples were obtained. The microstructures, mechanical properties, compressive strength, density values, and XRD-SEM results showed that the secondary phase Mg_2Ca increased with increasing Ca content, which indicates the increasing hardness of Mg-xCa alloy. Using the CCD method, the sample's compressive strength, hardness, and density results with optimal values produced from Mg-xCa alloys were determined as 251 MPa, 146 Brinell, and 1.7 g/cm^3, respectively. The compatibility of the experimental results with the Regression formula confirms the reliability of the equation.

Keywords: Powder metallurgy; CCD method; XRD; SEM-EDS; Mg-xCa alloys.

Submitted: January 30, 2025. **Accepted:** May 10, 2025.

Cite this: Güleryüz LF, İpek R. Microstructure-Mechanical Properties of Mg-xCa Alloys Produced by Mechanical Alloying-Hot Pressing Process and Their Optimization Using Central Composite Design Method. JOTCSA. 2025;12(2): 141-154.

DOI: https://doi.org/10.18596/jotcsa.1630114

***Corresponding author's E-mail:** ferayguleryuz@hotmail.com

1. INTRODUCTION

Central Composite Design (CCD) is a widely used five-level fractional factorial design, originally developed by Box and Wilson (1). The structure of CCD typically includes a 2^n full factorial design, 2 × n axial designs, and m central designs. In this setup, the axial designs are similar to the central designs, with the exception of one factor that takes levels either above the high level or below the low level of the 2^n full factorial design (2). One of the main advantages of CCD is its ability to estimate the nonlinearity of dependent variables effectively. Furthermore, it provides maximum information with a minimal amount of experimental data and reduces the number of experiments needed to predict quadratic terms in a second-order model. In addition to these benefits, CCD is highly effective in simultaneously evaluating mathematical and statistical data, making it a powerful tool for optimizing experimental conditions. This method enables researchers to manipulate multiple input factors at once and understand their individual and combined effects on a desired output. Due to these capabilities, CCD has become one of the most popular experimental designs in research fields that require precise modelling and optimization. Its efficiency and flexibility make it especially useful in developing predictive models and improving system performances with fewer experiments (6-9).

Mechanical alloying (MA) is a very widely used method in powder metallurgy production (10-12). Compared to other traditional metallurgical techniques, it is possible to produce alloys that are difficult to produce with the MA technique. Moreover, the MA method has an economic advantage since it enables the production of alloys with different

melting temperatures without reaching high temperatures (13). The powder metallurgy process is carried out in the solid state due to the absence or minimization of undesirable interface reactions between the matrix and the reinforcement element. Therefore, the MA method, which is a solid-state processing technique, is especially preferred in the production of magnesium matrix and calcium-reinforced alloys (14). The hexagonal close-packed structure of Mg (c/a = 1.624) forms solid solutions with many elements (15). Because the mechanical properties of alloying elements such as Mg can be further strengthened by solid solution, precipitation hardening, and grain refinement hardening (15), on the other hand, the superior properties of Mg–Ca alloys are reported (16), and their strength, surface corrosion, fatigue, biocompatibility, and allergic reaction properties of tissues are reported in different studies (17-20). Compared to traditional cold press sintering processes, the Joule sintering process is a process that minimizes porosity in the structure. The Joule heating technique requires a shorter time, less power, and a lower temperature. In addition, higher densities are obtained in this technique compared to cold press-sintering. Another advantage of this system is the sintering time, which does not require a long time as in other cold press processes (21-23).

In this study, the structural, morphological, and mechanical properties of Mg-xCa alloys produced by the mechanical alloying-hot pressing method were examined, and mechanical properties of Mg-xCa alloys produced by the mechanical alloying-hot pressing method were discussed, and statistical modeling was performed using the CCD method. Mg-xCa alloys with improved mechanical properties were successfully developed using the central composite design (CCD) method. The application of powder metallurgy and mechanical alloying at different times, followed by sintering at various temperatures, enabled precise control of microstructure and phase formation. The results showed that increasing Ca content promoted the formation of Mg_2Ca, leading to higher hardness and compressive strength. The strong correlation between the experimental results and the regression model confirmed the reliability of the CCD approach. The structural, morphological, and mechanical properties were determined using XRD, SEM-EDS analysis, and compressive strength-hardness tests.

2. EXPERIMENTAL

In the study, 9 different powder mixtures were prepared according to the CCD method for the mechanical alloying process, as seen in Table 1.

Table 1: Prepared mechanical alloying powders.

Sample no.	MA time (h)	Ca content (%)
Pure-Mg	0	0
1	11.99	4.7
2	14.43	2.7
3	14.43	6.7
4	18	1.33
5	18	4.7
6	18	8
7	21.57	2.7
8	21.57	6.7
9	24	4.7

The powders were subjected to a planetary ball milling process with 10 mm diameter stainless steel balls having 20:1 (ball/powder) weight ratio and 160 rpm rotation speed at different hours during mechanical milling. Then, a high-strength graphite mold with a 10 mm inner diameter and 60 mm height was used for the sample fast sintering process. Mg powder with 99% purity, an irregular grain shape, and an average grain size of 125 µm was used as reinforcement material, and calcium powder with 99.98% purity was used as matrix material. To prevent excessive cold welding, 2% by weight zinc stearate ($C_{36}H_{70}O_4Zn$) was added as a process control element in all samples. A mechanical alloying process was carried out to obtain Mg-xCa alloy.

Nine mechanically alloyed samples were subjected to a sintering process for 20 samples using five different temperatures according to CCD modeling. The ball-milled powders were placed in a graphite mold and hot press sintered under 46 Mpa pressure in an argon atmosphere. Different sintering temperatures (325-370-437-504-549 °C) and mechanical milling times (11.99-14.43-18-21.5-24 h) were carried out. Standard metallographic techniques were used to prepare the samples for microstructural examination. Metallographic samples were prepared from cross-sections of the investigated composites. All samples were gently ground.

In the CCD method, the selected factors are the Mg-xCa ratio, sintering temperature, and MA time. Independent variables are coded as -1 and +1, representing a two-level full factorial design. It has eight factorial points. The pivot point represents the high and low points of each factor. In the present study, CCD consists of $2k+2k+n$ runs. k is the number of factors. $2k$ is the number of factorial points, 2k is the number of axial points, α is the distance between the axial point and the center point, and α value is the coded value determined by the number of factors. It was obtained from the following Eq. (1):

$$\alpha = 2k^{1/2} \quad (1)$$

where the six axial points were located at (±α, 0, 0), (0, ±α, 0), (0, 0, ±α), and the six replicates were at the center (Figure 1).

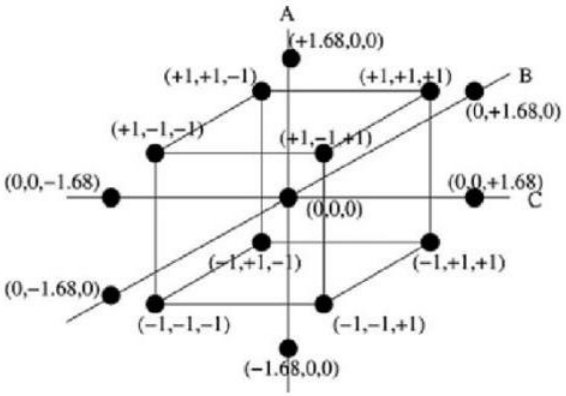

Figure 1: CCD design with 3 factors and 5 levels.

The phase structure of the samples was examined by XRD (X-ray diffractometer; D2 PHASER, Bruker Corp., Germany) using Cu-K_α (1.5406 Å) radiation in between 2θ=30-75 °C with scan speed 2 °C/min. The average crystallite sizes were determined from Scherrer Eq. (2) (24,25):

$$D = \frac{k \cdot \lambda}{\beta \cdot Cos\ \theta} \quad (2)$$

where D represents the crystallite size in nanometers, while k is considered a constant, typically valued at 0.9, CuKα denotes the wavelength (λ = 0.15406 Å), and β signifies the full width at half maximum measured in radians.

The surface morphology, microstructure, and phase detection of powders were performed by scanning electron microscopy (SEM; Jeol JSM 5910LV) equipped with energy dispersive spectroscopy (EDS; Oxford Instruments Inca X-Sight 7274). Hardness tests were performed on all samples using a Brinell hardness method with a 2.5 mm diameter ball indenter and 62.5 kgf load. For the compressing test, the cylindrical samples were determined by ASTM test method B 925-08 using a Zwick Roel Model 2100 tensile testing machine with a 0.5 mm/min testing speed.

3. RESULTS AND DISCUSSION

3.1. XRD-SEM Results of Mechanical Alloying Powders

Figure 2 shows the X-ray diffraction results of the powders after mechanical alloying. As seen in the XRD results, in addition to the Mg phase (JCPDS card no. 65-3583), a small amount of Mg_2Ca phase (JCPDS card no. 89-4244) was formed. Also, some MgO occurred due to the oxidation of Mg during MA. As seen in Figure 2, since mechanical alloying was done in an air environment, increasing the temperature with the milling time from 11.99 to 24 h increased the oxidation effect and, therefore, the MgO peak intensity in the XRD pattern. The mechanical alloying process ensures material homogenization and also leads to a reduction in grain size. From the XRD results, the crystallite size and Ca content-MA time relationship in the powders after the MA process were examined using the Scherrer equation, and the results are given in Table 2. While the initial grain size was 49 nm for pure Mg, it was found to be approximately 42 and 37 nm at 11.99 and 14.43 h MA times, respectively. The grain size continued to decrease and reached the lowest value of roughly 33 nm at the end of 18 h. The grain size tended to increase again after the 18 h MA process and was determined to be approximately 37 and 41 nm at 21.57 and 24 h MA times, respectively. During the MA process, grain growth is reported at long MA times (26-28), in which the dislocation mechanism is dominant at the beginning, and work hardening and temperature increase during MA effective. In addition, the present results showed that the duration of the mechanical alloying process is significantly effective compared to the Ca ratio.

Table 2: Crystallite sizes of mechanical alloying powders calculated from the Scherrer method and Ca amounts.

Sample no.	MA time (h)	Ca content (%)	Criystallite size (nm)
Pure-Mg	0	0	49
1	11.99	4.7	42
2	14.43	2.7	36
3	14.43	6.7	38
4	18	1.33	33
5	18	4.7	32
6	18	8	33
7	21.57	2.7	37
8	21.57	6.7	38
9	24	4.7	41

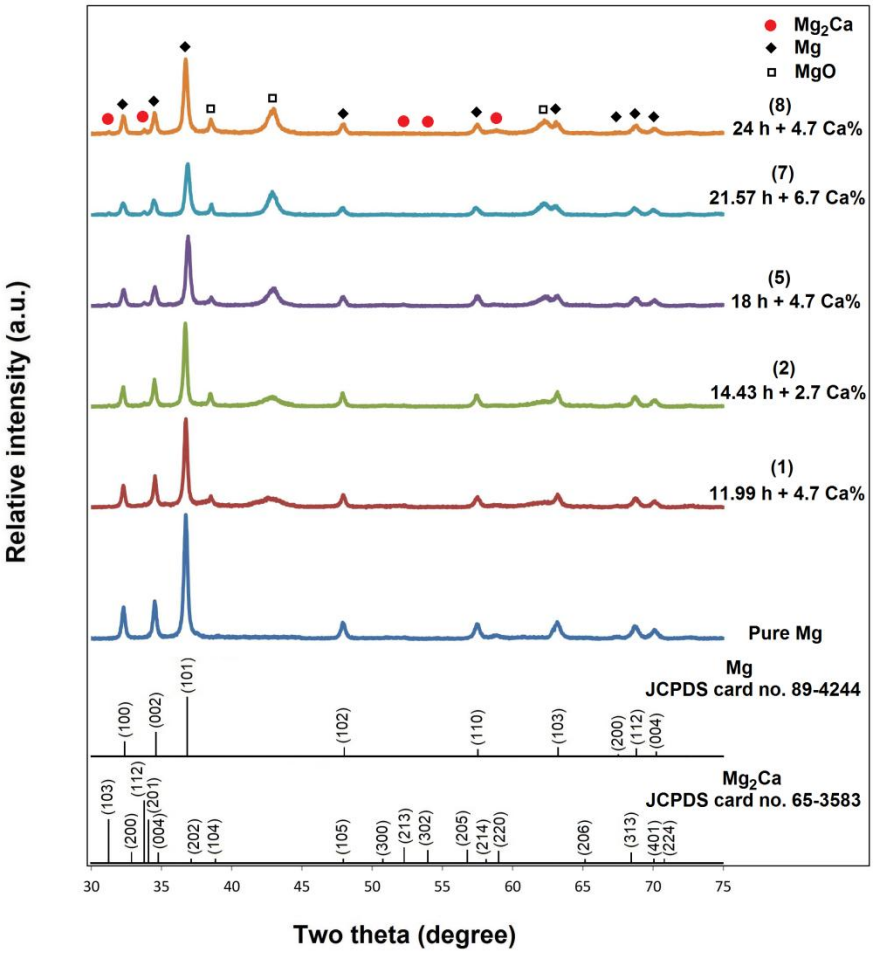

Figure 2: X-ray diffraction results of powders produced by adding Ca to pure Mg powder at different rates (between 1.33% and 8%) and performing MA for periods between 11.99 and 24 h.

Figure 3(a-e) shows the SEM images at x20000 magnification, showing the changes in the surface morphologies of the powders subjected to the mechanical alloying process at different MA times with different Ca contents. The SEM microstructure image of powder number 1 or code 4.7/11.99 is given in Figure 3a, where the grain shapes became significantly amorphous after 11.99 h mechanical grinding, consistent with the XRD result. In the SEM image of the 3-6.7/14.43 coded or powder number 3, whose MA time is 14.43 h and is given in Figure 3b, it was observed that the tendency for coalescence in the particles continued and the size decrease continued due to the shrinking amorphous particle structure. In Figure 3c, it was determined that the powder and grain sizes of the 4.7/18 coded powder number 5 subjected to an 18 h MA process were at the smallest values, which is the expected result of the grinding-boiling-breakage cycles in the mechanical grinding mechanism, in accordance with the literature. In addition, the breaking mechanism is effective here, and the grains are spherical. The powders given in Figure 3d and Figure 3e at 21.57 h (6.7/21.57 coded or powder number 7) and 24 h (4.7/24 coded or powder number 9) tended to cluster (plaque-like stratification) and grain growth was observed, respectively. It is seen from the SEM results that the agglomeration-clustering tendency continued to increase with the increase in grinding time. Additionally, the presence of Ca is likely to contribute to some tendency towards amorphization in the structure.

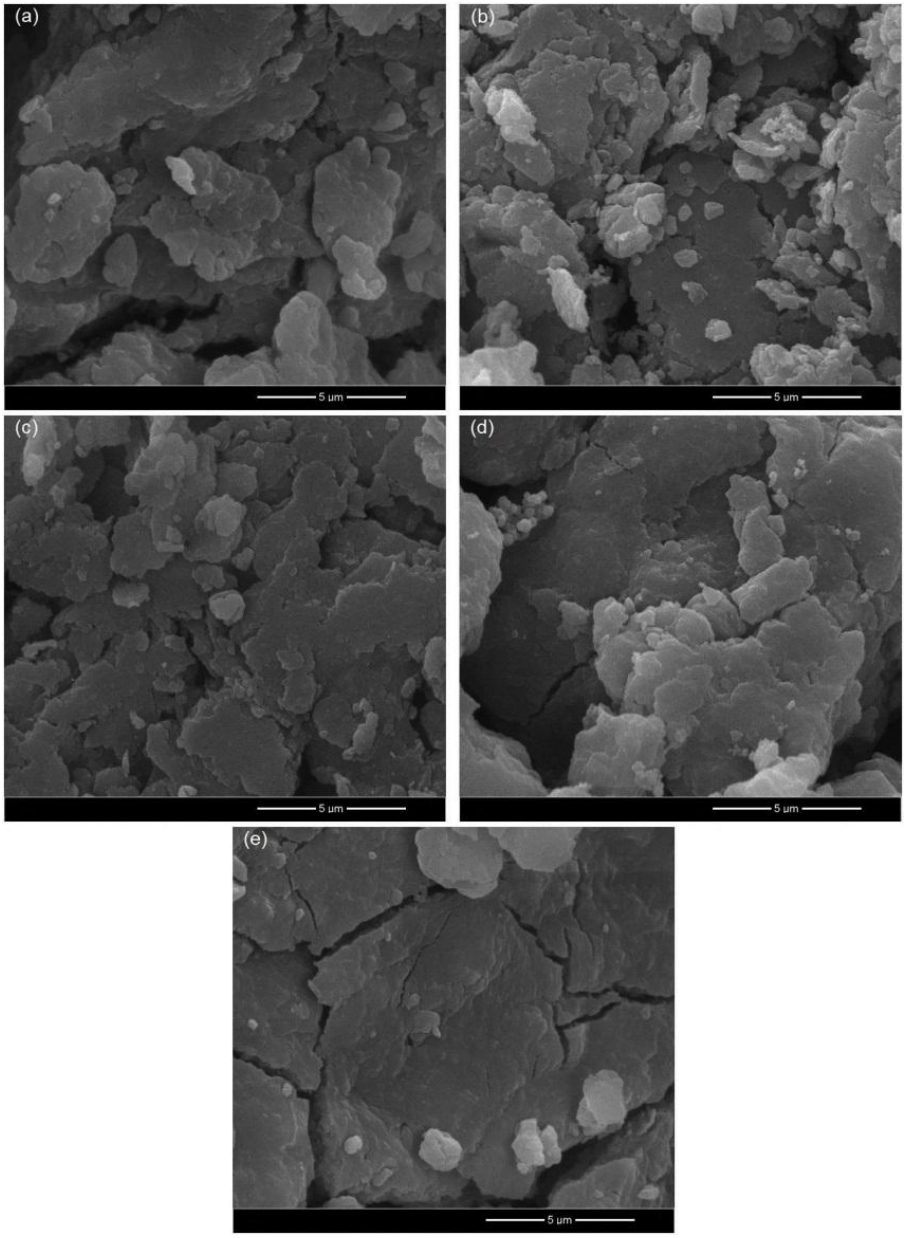

Figure 3: SEM micrographs at x20000 magnification of the powders mechanically alloyed at different times and Ca concentrations (a) 4.7/11.99, (b) 3-6.7/14.43, (c) 1-4.7/18, (d) 6-(6.7/21.57 and (e) 9-4.7/24, respectively.

3.2. XRD, SEM-EDS, Porosity, Mechanical Testing Results of Hot-Pressing Samples

The XRD results of the hot-pressing samples are given in Figure 4. As seen in the XRD results, in addition to the Mg main phase of the samples subjected to the sintering process at different temperatures, the Mg_2Ca phase formed during the MA process. In addition, as seen in Figure 4, the MgO phase formed during mechanical alloying is also present in the structure after the hot pressing process. While the broad MgO peaks in Figure 2 correspond to low crystallite size and amorphization, the sharpened peaks in Figure 4 can be associated with the crystallinity developing in the MgO phase and the increase in crystallite size.

Figure 5(a-f) shows the EDS results along with the SEM images for the hot-pressing samples. In the SEM images, the regions indicated by the red arrow indicate the regions where the Mg-xCa phase is present. The EDS results of the area where the entire SEM micrograph is scanned in Figure 5(a, b) and the blue framed region in Figure 5c are given in Figure 4d, e, and f, respectively. In EDS results, the Ca% contents of the samples vary between 2.65, 6.40, and 9.25% by weight and 1.49, 3.84, and 5.54 atomic % amounts, respectively. The theoretical contents of the samples have 1.33%, 4.7%, and 8% Ca, which are compatible with the amounts obtained as a result of elemental analysis, respectively. When the XRD and SEM-EDS results are evaluated together, the presence of oxygen in the EDS results is associated with some MgO phase in the Mg matrix formed during mechanical milling, as seen in the X-ray diffraction pattern. Moreover, depending on the presence of the Mg_2Ca phase in the XRD results, the grains with high atomic contrast in both the SEM backscattered electron images and the presence of the Ca element in the EDS results confirm the Mg_2Ca phase.

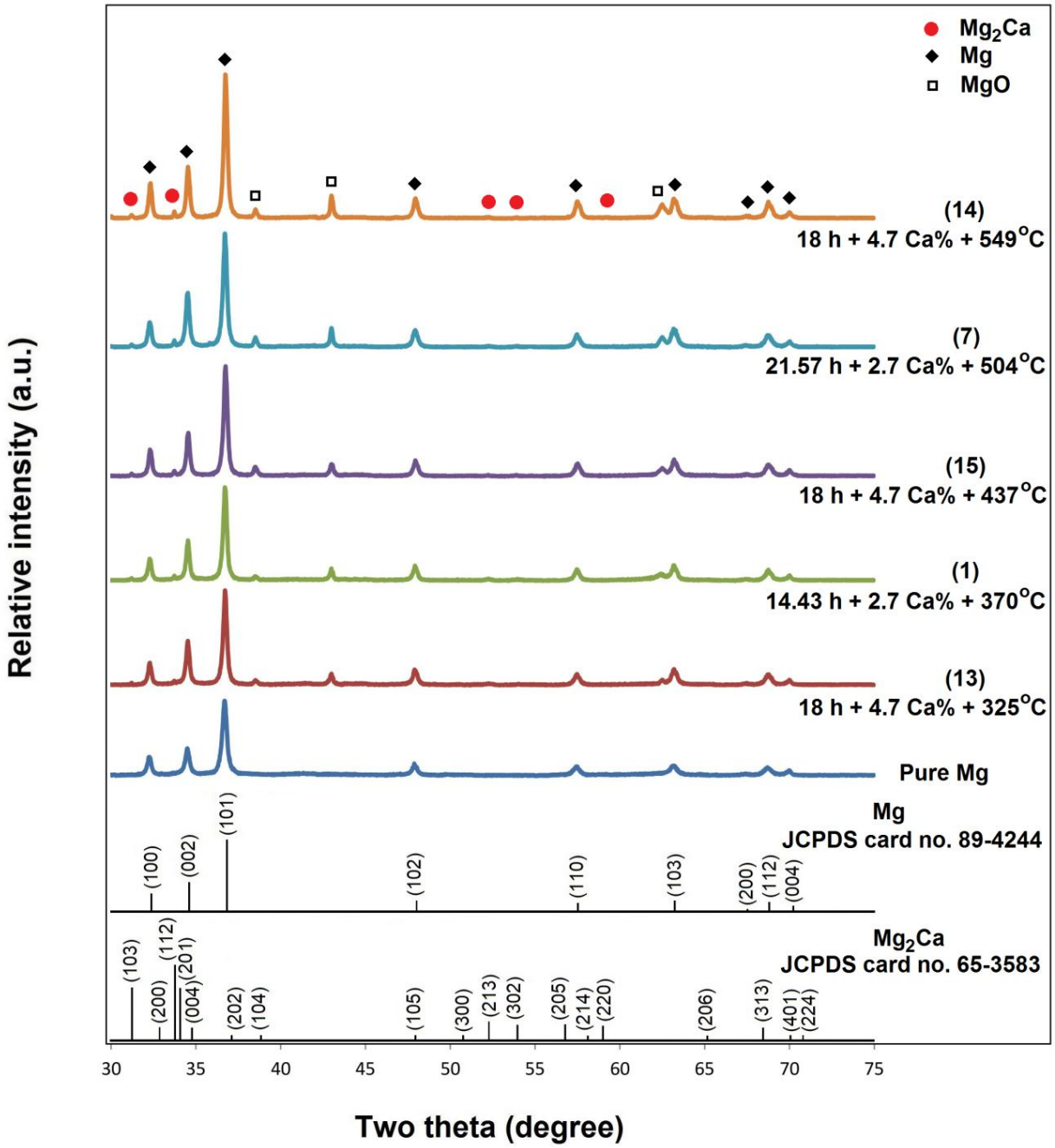

Figure 4: X-ray diffraction results of hot-pressing samples subjected to sintering at different temperatures.

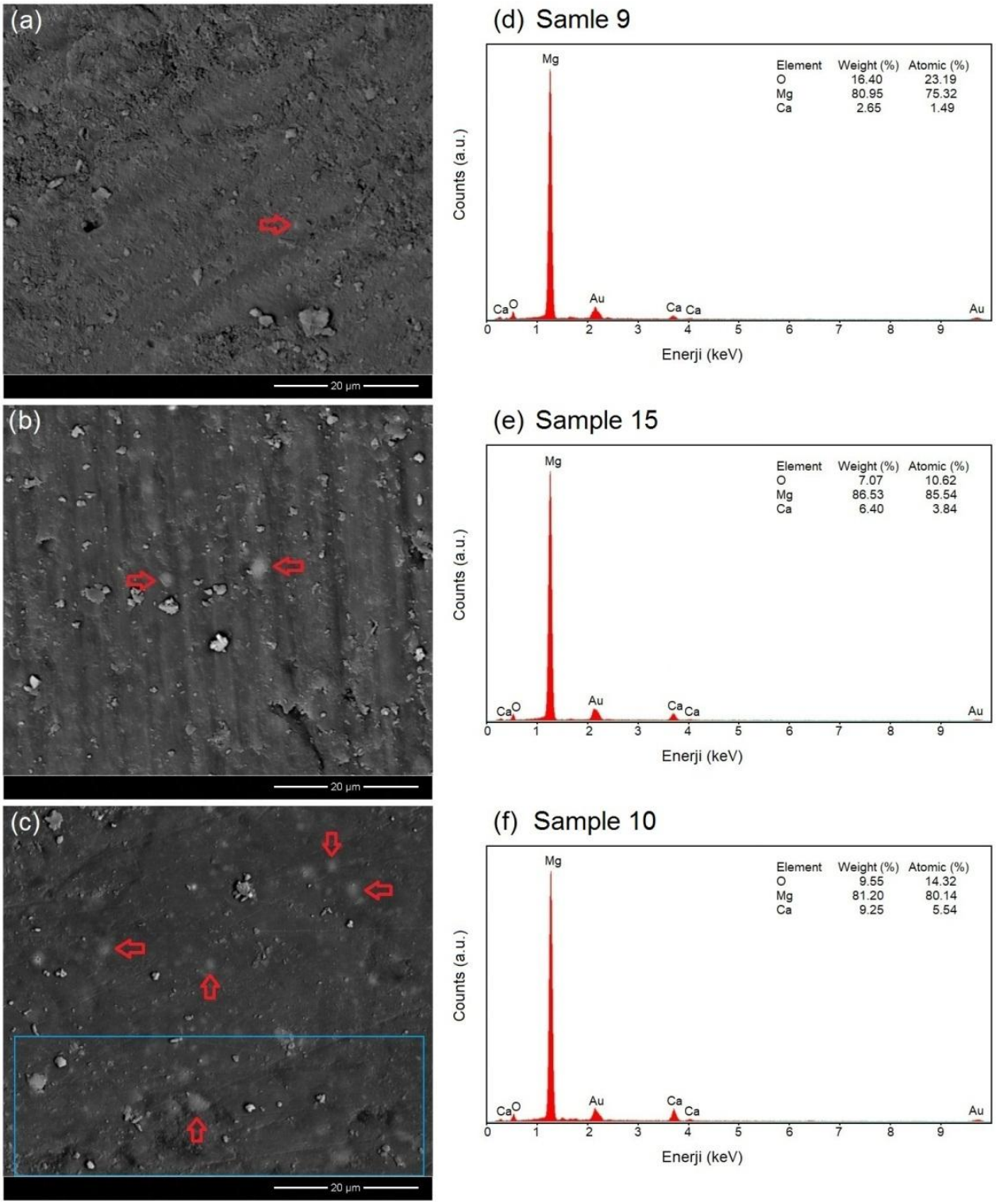

Figure 5: SEM (backscattered electron) images at x5000 magnification and EDS spectra for the hot-pressing samples (a)-(d) 1.33/18/437, (b)-(e) 4.7/18/437, (c)-(f) 8/18/437, respectively.

Theoretical, real densities and porosity amounts of hot-pressing samples are given in Table 3, where real densities and porosity amounts vary between 1.546-1.700 g/cm^3 and 1.6-11%, respectively. Compared with the theoretical values in Table 2, the actual densities and porosities of the samples vary depending on the Ca% ratio, MA time, and sintering temperature. The porosity results of the samples were examined based on the Ca ratio, MA time, and temperature factors and are given in Figure 6(a-c). The MA time reached the lowest porosity value around 18 h. At the same time, the Ca ratio showed a low porosity of 97, around 4.7%, where amounts above 4.7% Ca can be associated with an increase in the Mg_2Ca phase and deterioration in parameters. Another parameter, temperature, showed the lowest porosity around 437 °C (Figure 6c). Based on the obtained data, it is seen that the sintered samples achieved optimum porosity values at 18 h MA time, 4.7% Ca ratio, and 437 °C heat treatment temperature.

Table 3: Theoretical density, real density, and porosity results of hot-pressing samples.

Sample number	Sample code	Theoretical density-ρt (g/cm^3)	Real density-ρg (g/cm^3)	Porosity (%)
1	2.7/14.43/370	1.7329	1.609	7.1
2	6.7/14.43/370	1.7250	1.593	7.6
3	2.7/21.57/370	1.7329	1.603	7.5
4	6.7/21.57/370	1.7250	1.546	11
5	2.7/14.43/504	1.7329	1.643	5
6	6.7/14.43/504	1.7250	1.607	7
7	2.7/21.57/504	1.7329	1.655	4
8	6.7/21.57/504	1.7250	1.571	9
9	1.33/18/437	1.7350	1.690	3
10	8/18/437	1.7230	1.608	7
11	4.7/11.99/437	1.7290	1.569	10
12	4.7/24/437	1.7290	1.650	5
13	4.7/18/325	1.7290	1.615	7
14	4.7/18/549	1.7290	1.641	5
15	4.7/18/437	1.7290	1.682	2
16	4.7/18/437	1.7290	1.662	3
17	4.7/18/437	1.7290	1.666	3
18	4.7/18/437	1.7290	1.700	1.6
19	4.7/18/437	1.7290	1.690	2
20	4.7/18/437	1.7290	1.662	3

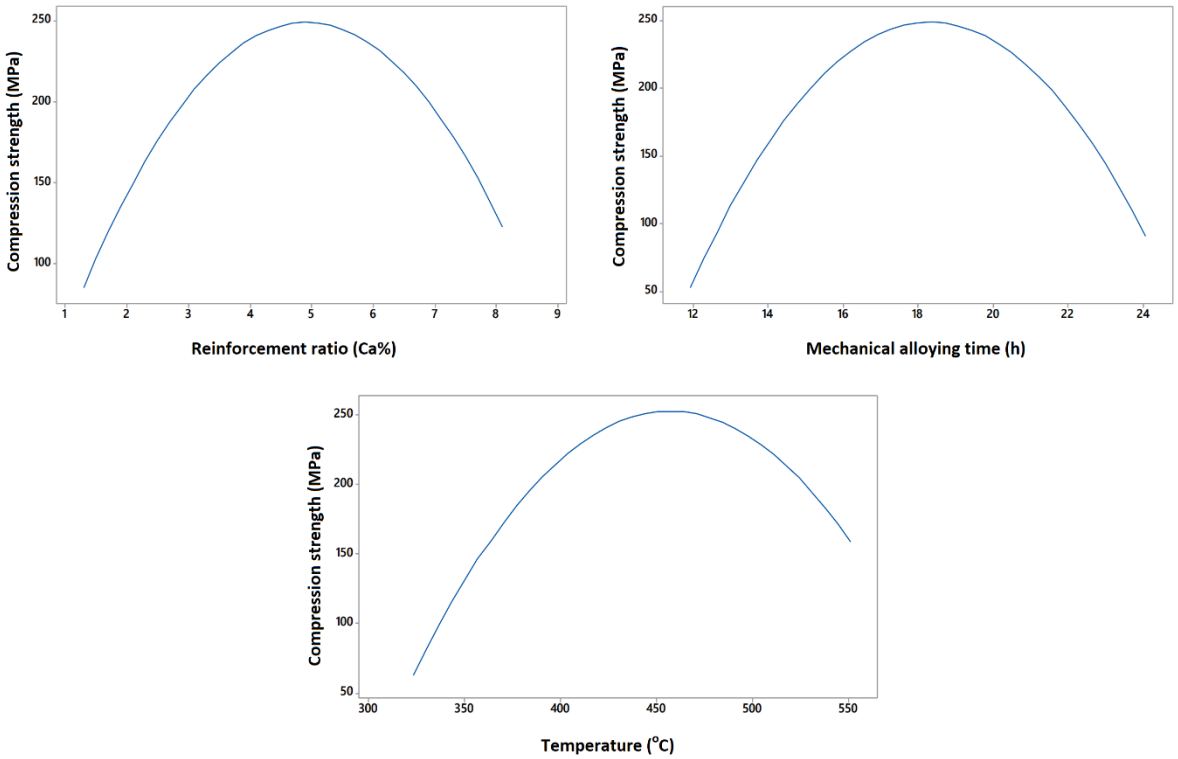

Figure 6: (a) %Ca ratio-porosity, (b) MA time-porosity, (c) Temperature-porosity results.

The hardness and compression test results of the samples subjected to hot pressing are summarized in Table 4. While the hardness values of the samples vary between 44-146 HB, the compression test values range between 38-251 MPa. In Table 4, it is seen that the hardness and compression test results are at high values for the sample with optimum values (sample coded 18-4.7/18/437), and these results are consistent with the literature data, which is given in Table 5. As seen in Table 5, in the study

conducted by Yahşi and İpek, compressive strength is 307 MPa for Mg/MgO structure after 18 h of milling and sintering at 550 °C (29). In another study by Hirata et al., compressive strength is 150 MPa for Al_2O_3 alloy after 24 h milling time and 1300 °C sintering (30). Yahşi et al. (31) reported compressive strength values of 195 and 192 MPa, respectively, at short milling times by adding 10% and 20% of PVA (polyvinyl alcohol) to the Mg matrix.

Table 4: Brinell hardness and compressive strength results of hot-pressing samples.

Sample number	Sample code	Brinell hardness (kg/mm^2)	Compressive strength (MPa)
1	2.7/14.43/370	44	38
2	6.7/14.43/370	52	39
3	2.7/21.57/370	52	76
4	6.7/21.57/370	45	108
5	2.7/14.43/504	108	94
6	6.7/14.43/504	91	132
7	2.7/21.57/504	69	75
8	6.7/21.57/504	60	116
9	1.33/18/437	127	102
10	8/18/437	123	125
11	4.7/11.99/437	58	58
12	4.7/24/437	46	106
13	4.7/18/325	49	52
14	4.7/18/549	131	188
15	4.7/18/437	143	250
16	4.7/18/437	143	245
17	4.7/18/437	145	249
18	4.7/18/437	146	251
19	4.7/18/437	144	245
20	4.7/18/437	143	220

Table 5: Study results and literature data.

MA time (h)	Sintering temperature (C^o)	Matrix	Additive	Content (%)	Brinell hardness (kg/mm^2)	Compressive strength (MPa)	Ref.
18	437	Mg	Mg	4.7	146	251	This study
18	550	Mg	Mg	-	35	307	(29)
24	1300	AKP50	AKP20	1-100	-	150	(30)
0.5	400	Mg	PVA	10	-	195	(31)
1	400	Mg	PVA	20	-	192	(31)

3.3. Evaluation of Hot-Pressing Samples with Statistical Model Central Composite Design (CCD) Method

Table 6 presents the regulated version of the samples produced according to different Ca% (X1), MA (X2), and temperature (X3) parameters according to the CCD experimental design method.

To determine the experimental factors (A, B, C) and the interactions between the factors (A*A, B*B, C*C, A*B, A*C, B*C) and to test the reliability of the experiments, ANOVA analysis was performed using the data in Table 6 with the help of the Minitab 17 program. The results obtained are summarized in Table 7.

Table 6: Regulation of hardness, porosity, and compressive strength parameters of hot-pressing samples according to CCD method.

Std. ord.	Run ord.	Coded Variables			Uncoded Variables			Hardness (HB)	Porosity (%)	Comp. Strength (MPa)
		X1	X2	X3	X1	X2	X3			Y
1	1	-1	-1	-1	2.7	14.43	370	44	7.1	38
2	7	1	-1	-1	6.7	14.43	370	52	7.6	39
3	16	-1	1	-1	2.7	21.57	370	52	7.5	76
4	12	1	1	-1	6.7	21.57	370	45	11	108
5	9	-1	-1	1	2.7	14.43	504	108	5	94
6	2	1	-1	1	6.7	14.43	504	91	7	132
7	20	-1	1	1	2.7	21.57	504	69	4	75
8	8	1	1	1	6.7	21.57	504	60	9	116
9	13	-1.68179	0	0	1.33	18	437	127	3	102
10	19	1.68179	0	0	8	18	437	123	7	125
11	11	0	-1.68179	0	4.7	12	437	58	10	58
12	3	0	1.68179	0	4.7	24	437	46	5	106
13	5	0	0	-1.68179	4.7	18	325	49	7	52
14	18	0	0	1.68179	4.7	18	549	131	5	188
15	10	0	0	0	4.7	18	437	143	2	250
16	17	0	0	0	4.7	18	437	143	3	245
17	15	0	0	0	4.7	18	437	145	3	249
18	14	0	0	0	4.7	18	437	146	1.6	251
19	4	0	0	0	4.7	18	437	144	2	245
20	6	0	0	0	4.7	18	437	143	3	220

Table 7: ANOVA analysis of hot-pressing samples.

Analysis of variance (ANOVA) of CCD model					
Source	Degrees of Freedom (DF)	Sum of squares	Mean square	F value	P value
MODEL	9	114047	12671.9	42.81	0.000 significant
LINEAR	3	14208	4736.1	16.00	0.000
A	1	1663	1662.5	5.62	0.039
B	1	1708	1708.0	5.77	0.037
C	1	10838	10838.0	36.61	0.000
SQUARE	3	96909	32303.0	109.13	0.000
A*A	1	33819	33819.0	114.25	0.000
B*B	1	51156	51156.4	172.82	0.000
C*C	1	30686	30686.4	103.67	0.000
2-Way interaction	3	2930	976.5	3.30	0.066
A*B	1	145	144.5	0.49	0.501
A*C	1	264	264.5	0.89	0.367
B*C	1	2521	2520.5	8.52	0.015
Resudial error	10	2960	296.0		
Lack of fit	5	2275	454.9	3.32	0.107 significant
Pure error	5	685	137.1		
Total	19	117007			
R-sq	97.47 %				

In Table 7, when the model is evaluated in terms of F and P-value, the model created is statistically significant because the P-value for the F-value of 42.81 is less than 0.05 (0.000<0.05). On the other hand, when the model is evaluated in terms of Lack of fit and P-value, it is not significant because the lack of fit is 0.107>0.05. The lack of fit test determines whether the mathematical form of the obtained model is suitable for representing the experimental data (32). As a result, the lack of fit value is insignificant in the adjusted model. Therefore, the removal of two-way interactions (A*B,

A*C, B*C) components in Table 7 does not affect the model reliability.

Table 8: ANOVA analysis result data.

Adeq-precision	16.7556
R-Sq	%97.12
R-Sq (adj)	%95.44
R-Sq(pred)	%88.50

In Table 8, Adeg-precision measures the signal/noise ratio, which becomes significant when it is greater than 4. For this model, Adeg-precision=16.7556 is a suitable value and shows a sufficient signal/noise ratio. RSq value and RSq (adj) values are 97.12% and 95.44%, respectively. The R Sq value is close to 97.12%, indicating that the deviation in the distribution of the experiments is low. The RSq (adj) value is 95.44%. The R Sq (pred) value is expected to be close to RSq (adj), and 88.5% is a reasonable value. As a result, when all three parameters are considered, the most effective factor is temperature. In addition, the MA-temperature interaction is relatively more effective than the MA-Ca ratio and the temperature-Ca ratio. The following Regression Eq. (3) was obtained using the Minitab 17 program.

$$C8 = 243.72+11.03*A + 11.18*B + 28.17\ C - 48.44\ A*A - 59.58\ B*B - 46.14\ C*C - 17.75\ B*C \quad (3)$$

The regression equation is 97.80%. R-Sq (adj) value is 95.44% and close to 97.80%. Here, C8 gives the estimated value. A, B, and C show the coded factors. The (+) values seen here show that the increase in reinforcement ratio, MA time, and temperature increases the compressive strength. It is seen that the most effective of the main factor values is temperature. It is understood that the interaction between the factors (A*A, B*B, C*C) is more effective than the main effects (A, B, C). The regression Eq. (3) confirms that it can be used to estimate compressive strength within the limit values. The comparison of the experimental results according to the regression equation is shown in the graph in Figure 7. As seen in the graph, the experimental results are in good agreement with the results calculated according to the Regression equation.

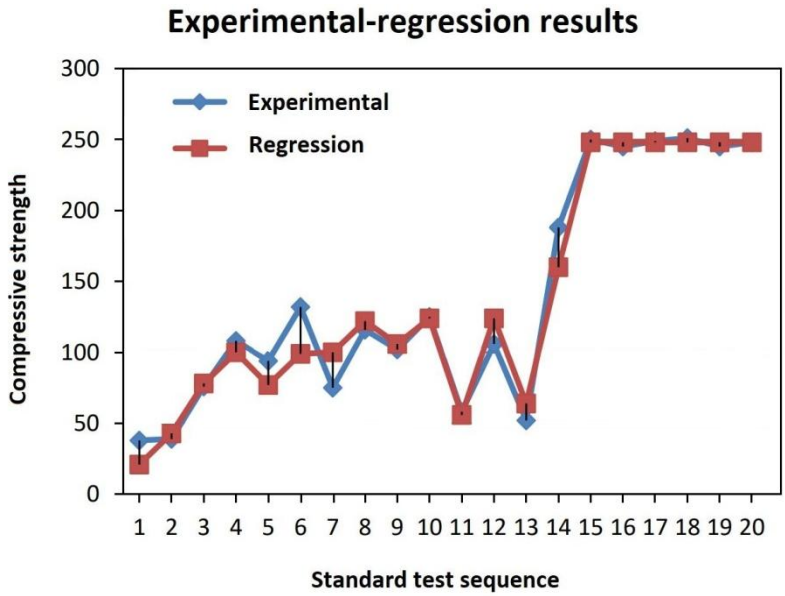

Figure 7: Regression equation and experimental results comparison graph.

4. CONCLUSION

In this study, the mechanical performance of Mg-xCa alloys was systematically investigated by applying the Central Composite Design (CCD) methodology. CCD enabled the optimization and prediction of mechanical properties by controlling two critical process parameters: mechanical alloying time and sintering temperature, where Mg and Ca powders were subjected to mechanical alloying for varying durations (11.99, 14.43, 18, 21.5, and 24 hours), followed by sintering at different temperatures (325°C, 370°C, 437°C, 504°C, and 549°C) under an argon atmosphere at 46 MPa pressure. XRD, SEM-EDS analyses, and grain size measurements revealed that prolonged alloying time and higher sintering temperatures promoted the formation of the Mg_2Ca secondary phase. The presence of this phase contributed significantly to the enhancement of mechanical properties. The experimental results indicated a clear increase in compressive strength, hardness, and density with increasing Ca content. The maximum compressive strength, hardness, and density obtained were 251 MPa, 146 Brinell hardness, and 1.7 g/cm^3, respectively. Using the CCD model, regression equations were derived that accurately predicted the experimental outcomes. The close correlation between the experimental data and the model predictions validated the reliability of the CCD approach in optimizing the mechanical performance of Mg-xCa alloys. Moreover, the findings confirm that fine-tuning processing parameters through statistical modelling can significantly enhance the mechanical behavior of magnesium-based alloys produced by powder metallurgy. This study demonstrates that CCD is an effective and reliable method for process optimization in developing high-performance Mg

alloys with controlled degradation rates, which is crucial for biomedical and structural applications.

5. CONFLICT OF INTEREST

There is no conflict of interest.

6. REFERENCES

1. Box GEP, Wilson KB. On the experimental attainment of optimum conditions. In: Kotz S, Johnson NL, editors. Breakthroughs in Statistics [Internet]. Springer, New York, NY; 1992. p. 270–310. Available from: <URL>.

2. Kuehl RO. Design of experiments: statistical principles of research design and analysis. Duxbury Press; 2000.

3. Wang J, Wan W. Experimental design methods for fermentative hydrogen production: A review. Int J Hydrogen Energy [Internet]. 2009 Jan;34(1):235–44. Available from: <URL>.

4. Li Z, Lu D, Gao X. Optimization of mixture proportions by statistical experimental design using response surface method - A review. J Build Eng [Internet]. 2021 Apr;36:102101. Available from: <URL>.

5. O-Thong S, Prasertsan P, Intrasungkha N, Dhamwichukorn S, Birkeland NKå. Optimization of simultaneous thermophilic fermentative hydrogen production and COD reduction from palm oil mill effluent by *Thermoanaerobacterium*-rich sludge. Int J Hydrogen Energy [Internet]. 2008 Feb;33(4):1221–31. Available from: <URL>.

6. Mohapatra S, Pradhan N, Mohanty S, Sukla LB. Recovery of nickel from lateritic nickel ore using *Aspergillus niger* and optimization of parameters. Miner Eng [Internet]. 2009 Feb;22(3):311–3. Available from: <URL>.

7. Solanki N, Saini S, Singh SK, Paudel KR, Goh BH, Dua K, et al. Central composite designed boswellic acids loaded nanoparticles for enhanced cellular uptake in human lung cancer cell line A549. J Drug Deliv Sci Technol [Internet]. 2025 Mar;105:106591. Available from: <URL>.

8. Ndlovu A, Cornish LA, Sithebe HSL. Relationship between sintering pressure and leach rate of polycrystalline diamond compacts (PDCs) using central composite design (CCD) modelling. Int J Refract Met Hard Mater [Internet]. 2024 Nov;124:106854. Available from: <URL>.

9. Verma S, Verma B. Optimizing carbon nanotube-doped ternary composite for high-energy-density hybrid supercapacitors: A comprehensive electrochemical assessment through central composite design. J Ind Eng Chem [Internet]. 2024 Dec;140:354–63. Available from: <URL>.

10. Zhao H, Wang W, Fu Z, Wang H. Thermal conductivity and dielectric property of hot-pressing sintered AlN–BN ceramic composites. Ceram Int [Internet]. 2009 Jan;35(1):105–9. Available from: <URL>.

11. İlhan M, Mergen A, Yaman C. Removal of iron from $BaTa_2O_6$ ceramic powder produced by high energy milling. Ceram Int [Internet]. 2013 Jul;39(5):5741–50. Available from: <URL>.

12. İlhan M, Mergen A, Yaman C. Mechanochemical synthesis and characterisation of $BaTa_2O_6$ ceramic powders. Ceram Int [Internet]. 2011 Jul;37(5):1507–14. Available from: <URL>.

13. Suryanarayana C, Ivanov E, Boldyrev V. The science and technology of mechanical alloying. Mater Sci Eng A [Internet]. 2001 May;304–306:151–8. Available from: <URL>.

14. Song SG, Shi N, Gray GT, Roberts JA. Reinforcement shape effects on the fracture behavior and ductility of particulate-reinforced 6061-Al matrix composites. Metall Mater Trans A [Internet]. 1996 Nov;27(11):3739–46. Available from: <URL>.

15. Bamberger M, Dehm G. Trends in the development of new Mg alloys. Annu Rev Mater Res [Internet]. 2008 Aug 1;38(1):505–33. Available from: <URL>.

16. Li Z, Gu X, Lou S, Zheng Y. The development of binary Mg–Ca alloys for use as biodegradable materials within bone. Biomaterials [Internet]. 2008 Apr;29(10):1329–44. Available from: <URL>.

17. Bronzino JD. Medical devices and systems, the biomedical engineering handbook [Internet]. Bronzino JD, editor. CRC Press; 2006. Available from: <URL>.

18. Park JB, Lakes RS. Biomaterials [Internet]. New York, NY: Springer New York; 2007. Available from: <URL>.

19. Chen Y, Xu Z, Smith C, Sankar J. Recent advances on the development of magnesium alloys for biodegradable implants. Acta Biomater [Internet]. 2014 Nov;10(11):4561–73. Available from: <URL>.

20. Zberg B, Uggowitzer PJ, Löffler JF. MgZnCa glasses without clinically observable hydrogen evolution for biodegradable implants. Nat Mater [Internet]. 2009 Nov 27;8(11):887–91. Available from: <URL>.

21. Carney CM, Mah T. Current isolation in spark plasma sintering of conductive and nonconductive ceramics. J Am Ceram Soc [Internet]. 2008 Oct;91(10):3448–50. Available from: <URL>.

22. Song X, Liu X, Zhang J. Neck formation and self-adjusting mechanism of neck growth of conducting powders in spark plasma sintering. J Am Ceram Soc [Internet]. 2006 Feb 14;89(2):494–500. Available from: <URL>.

23. Jha SK, Raj R. The effect of electric field on sintering and electrical conductivity of titania. Chen I -W., editor. J Am Ceram Soc [Internet]. 2014 Feb 13;97(2):527–34. Available from: <URL>.

24. İlhan M, Ekmekçi MK, Güleryüz LF. Effect of boron incorporation on the structural, morphological, and spectral properties of $CdNb_2O_6:Dy^{3+}$ phosphor synthesized by molten salt process. Mater Sci Eng B [Internet]. 2023 Dec;298:116858. Available from: <URL>.

25. İlhan M, Güleryüz LF, Ekmekci MK. Structural properties, photoluminescence, and judd-ofelt parameters of Eu^{3+}-doped $CoNb_2O_6$ phosphor. J Turkish Chem Soc Sect A Chem [Internet]. 2023 Aug 30;10(3):745–56. Available from: <URL>.

26. Yoon KH, Park HS, Cho JY, Kim ES. Microwave dielectric properties of $(Pb_{0.4}Ca_{0.6})(Fe_{0.5}Ta_{0.5})O_3$ ceramics prepared by mechanochemical processing. J Eur Ceram Soc [Internet]. 2003 Jan;23(14):2579–82. Available from: <URL>.

27. Mergen A. Mechanochemical synthesis of $MgTa_2O_6$ ceramic. Ceram Int [Internet]. 2009 Apr;35(3):1151–7. Available from: <URL>.

28. Moure A, Castro A, Tartaj J, Moure C. Mechanosynthesis of perovskite $LaGaO_3$ and its effect on the sintering of ceramics. Ceram Int [Internet]. 2009 Sep;35(7):2659–65. Available from: <URL>.

29. Yahşi Y, İpek R. Effect of ball milling time on microstructural properties of Mg/MgO. Hacettepe J Biol Chem [Internet]. 2022 Aug 1;50(3):269–74. Available from: <URL>.

30. Hirata Y, Fujita H, Shimonosono T. Compressive mechanical properties of partially sintered porous alumina of bimodal particle size system. Ceram Int [Internet]. 2017 Feb;43(2):1895–903. Available from: <URL>.

31. Yahsi Y, Yusan S, Akgol S, Ipek R. Experimental investigation of sinterability of PVA-coated Magnesium powders via mechanical milling using electric field-assisted sintering technique. Kov Mater Mater [Internet]. 2024 Nov 6;62(4):211–22. Available from: <URL>.

32. Myers RH, Montgomery DC. Response surface methodology: Process and product optimization using designed experiment [Internet]. John Wiley & Sons. Inc.; 1995. Available from: <URL>.